analytical chemistry

pubs.acs.org/ac Article

Glycoproteomic Analysis of Human Urinary Exosomes

Christopher J. Brown, Stefan Gaunitz, Ziyu Wang, Lena Strindelius, Stephen C. Jacobson, David E. Clemmer, Jonathan C. Trinidad,* and Milos V. Novotny*

Cite This: *Anal. Chem.* 2020, 92, 14357−14365 Read Online

ACCESS | Metrics & More | Article Recommendations | Supporting Information

ABSTRACT: Exosomes represent a class of secreted biological vesicles, which have recently gained attention due to their function as intertissue and interorganism transporters of genetic materials, small molecules, lipids, and proteins. Although the protein constituents of these exosomes are often glycosylated, a large-scale characterization of the glycoproteome has not yet been completed. This study identified 3144 unique glycosylation events belonging to 378 glycoproteins and 604 unique protein sites of glycosylation. With these data, we investigated the level of glycan microheterogeneity within the urinary exosomes, finding on average 5.9 glycans per site. The glycan family abundance on individual proteins showed subtle differences, providing an additional level of molecular characterization compared to the unmodified proteome. Finally, we show protein site-specific changes in regard to the common urinary glycoprotein, uromodulin. While uromodulin is an individual case, these same site-specific analyses provide a way forward for developing diagnostic glycoprotein biomarkers with urine as a noninvasive biological fluid. This study represents an important first step in understanding the functional urinary glycoproteome.

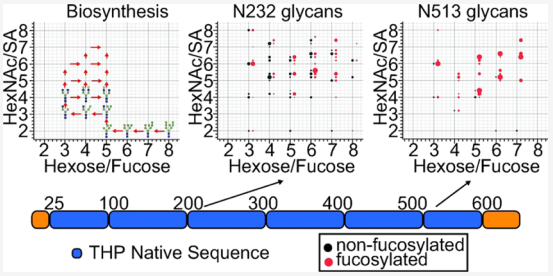

INTRODUCTION

Exosomes are an important set of secreted vesicles that transport small molecules, lipids, genetic materials, and proteins between tissues[1,2] and organisms.[3,4] These vesicles are able to target particular tissues or cells by utilizing surface proteins for cellular recognition, leading to endocytosis and deposition of functional cargo into the target cell. In addition to those features, exosomes have also been shown to cross biological barriers (e.g., the blood−brain barrier), making them an attractive carrier for targeted drug delivery.[5,6] These extracellular vesicles have also been investigated as potential disease diagnostics. Because a large number of cell types are known to secrete these vesicles, exosomes have the potential to report on tissues that would otherwise require invasive procedures. This ability to analyze materials such as blood or urine, collected remotely from the tissue of interest, has recently been coined "liquid biopsy" and represents a fast-growing field.[7−9]

Urine is an abundant and accessible biological fluid used to study changes in human physiology. While urine analysis typically focuses on measuring changes in metabolites or protein levels, analyzing protein glycosylation provides an additional metric into the physiological state of the cells from which these proteins were secreted. Glycoproteome analysis of urinary proteins is less straightforward than analysis of the serum glycoproteome. Urinary protein levels are much lower than those in blood due to filtering by the kidney glomeruli. One of the most abundant urinary proteins is uromodulin, also known as the Tamm−Horsfall protein (THP), which is found at a concentration of approximately 4.5 μg/mL.[10] This protein creates "webs" of aggregates that trap exosome vesicles, and as a consequence, THP is present in urine exosome preparations despite not being a principal exosome component. Additionally, THP is heavily glycosylated. These aspects of THP pose a unique analytical challenge with regard to both the release and isolation of exosomes as well as the subsequent enrichment of their relevant glycoproteins.

Glycosylation is one of the most abundant protein post-translational modifications (PTMs), affecting the majority of transmembrane and secreted proteins. Because of the biological importance of glycosylation, many recent publications have investigated technologies to enrich and identify these PTMs.[11,12] Many of these technologies have focused on the glycomic identification of the released glycans[13−15] or identification of deglycosylated peptides,[16,17] thereby simplifying the analysis. Although the study of the isolated moiety (i.e., glycan or peptide) can provide useful information, the analysis of the intact PTM provides a more detailed view of the protein.[12]

In this manuscript, the glycoproteome of human urinary exosomes was investigated with multilectin affinity chromatography and mass spectrometry. We identified 3565 glycopeptides from 378 glycoproteins. Removing redundancies due to

Received: May 6, 2020
Accepted: September 28, 2020
Published: September 28, 2020

https://dx.doi.org/10.1021/acs.analchem.0c01952
Anal. Chem. 2020, 92, 14357−14365

issues such as missed proteolytic cleavage sites and variable peptide oxidation gave a total of 3144 unique glycosylation events defined as a unique protein, modification position, and glycan. The level of glycan microheterogeneity (5.9 glycans per site) was measured for 604 unique protein glycosylation sites. Low-abundance proteins showed comparably fewer sites of glycosylation; however, glycoproteins below the limit of detection for standard proteome analysis were identified upon enrichment (n = 120). Specific glycoforms were identified that span the range of glycoprotein abundance (based on the summed number of glycopeptide identifications), whereas other glycoforms were only found on high-abundance proteins. Proteins with multiply identified sites of glycosylation showed a wide variation in the glycoform composition between those sites. For example, uromodulin displayed significantly different glycoform patterns at different sites across the protein. These observations represent an important first step in better characterizing the glycoproteome of these exosome species.

MATERIALS AND METHODS

Sample Collection. Urine was isolated from consenting males under the procedures outlined by the Indiana University protocol IUSCC-0588. A total of approximately 800 mL of urine was collected over several mornings with an average of 80 mL per collection. Single tablets of cOmplete protease inhibitor cocktail (Sigma-Aldrich, St. Louis, MO) and 0.01% sodium azide in water (Sigma-Aldrich, St. Louis, MO) were added to each 40 mL aliquot of urine. The urine samples were stored at 4 °C and used within 24 h of collection.

Differential Ultracentrifugation. The samples were processed similarly to Zou et al., with slight modifications.[13] The urine samples (40 mL each) from two individuals were processed in parallel and pooled prior to ultracentrifugation. They were subsequently centrifuged at 17 000g for 1 h (JA-17 fixed angle rotor) at 20 °C to remove urinary sediment, cell debris, membrane, and THP protein aggregates. The supernatant (SN1) was retained for later ultracentrifugation steps. The pellet was resolubilized with 500 μL of isolation solution (10 mM triethanolamine, 250 mM sucrose, pH 7.0). The resolubilized pellet was then incubated with 500 μL of 200 mg/mL d-dithiothreitol (Bio-Rad, Hercules, CA) for 45 min at 37 °C, with brief vortexing every 15 min to reduce disulfide bonds. The reduced samples were then centrifuged at 14 000g (Eppendorf Centrifuge 5424, Eppendorf AG, Hamburg, Germany) for 7 min at room temperature. The supernatant was combined with SN1 and stored for no more than 24 h at 4 °C. The combined supernatant was transferred to ultracentrifuge tubes and centrifuged at 200 000g with an Optima XPN, Rotor: 70.1 Ti (Beckman-Coulter, Indianapolis, IN) for 1 h at room temperature. The supernatant was discarded, and the pellet was resolubilized in 1× PBS buffer. An additional centrifugation was performed to repellet the material at 200 000g. The supernatant was again discarded and the pellet was resolubilized in 8 M urea (Sigma-Aldrich, St. Louis, MO) in 100 mM ammonium bicarbonate (Sigma-Aldrich, St. Louis, MO). This process resulted in approximately 5 mg of the protein material. The samples were briefly vortexed and then stored at −80 °C until digestion.

Protein Digestion. The samples were concentrated through a 30 kDa, Amicon Ultra-15 molecular weight cut off filter (Millipore, Burlington, MA) based on the method of Wisniewski.[18] While this may lead to some loss of proteins below 30 kDa, in our final list we nevertheless identified glycopeptides from 38 proteins below this cutoff. The samples were subsequently reduced with 2 mM tris(2-carboxyethyl)-phosphine hydrochloride (Sigma-Aldrich, St. Louis, MO) for 1 h at 56 °C. The reduced proteins were allowed to react with 4 mM iodoacetamide (Sigma-Aldrich, St. Louis, MO) for 45 min in the dark at room temperature to alkylate cysteine residue side chains. The urea concentration was diluted to 1 M with 100 mM pH 7.5 ammonium bicarbonate (Sigma-Aldrich, St. Louis, MO) and modified sequencing grade trypsin (Promega, Madison, WI) was added at a 1:100, enzyme:protein ratio. Trypsin digestion occurred overnight at 37 °C. After digestion, the peptides were desalted with C-18 preparative Sep-Pak (Waters, Milford, MA). A small aliquot of this sample was reserved for proteomic analysis prior to glycopeptide enrichment.

Enrichment and Fractionation. The desalted peptides were then dried and resolubilized in lectin weak affinity chromatography (LWAC) buffer (100 mM tris-base, pH 7.6, 50 mM NaCl, 2 mM $CaCl_2$). The aliquots (0.5 mg) were loaded onto a multilectin enrichment column and separated at 200 μL/min. The nonglycosylated peptides eluted in the unbound flow-through peak. The bulk of this initial peak was diverted to waste. The glycopeptides have been previously determined to begin eluting as the rightward tail of this peak decreased to approximately 10% of the peak height. At this time, a 2.8 mm × 2 cm trapping column (IDEX-HS, Oak Harbor, WA) packed with POROS 20 R2 resin (Thermo Fisher, Waltham, MA) was switched online downstream to capture the eluent. Each aliquot was sequentially added, and the glycosylated fraction was trapped. Following enrichment of the final aliquot, the LWAC column was switched off-line, the trap column was desalted with separation buffer of 20 mM ammonium formate, pH 10.0 (Thermo Fisher, Waltham, MA), and a 150 × 2.1 mm^2 Kinetex 5 μm EVO C18 100 Å analytical column (Phenomenex, Torrance, CA) was switched online. The peptides were eluted over a 14 mL gradient from 0 to 60% B (20 mM ammonium formate, 80% acetonitrile, 20% water, pH 10, Thermo Fisher, Waltham, MA). The peptides were collected in fractions with a volume between 0.2 and 0.3 mL, depending on the location within the run. A total of 23 peptide fractions were collected and dried to completeness.

Mass Spectrometry Analysis. The dried fractions were resolubilized in low pH buffer A containing 0.1% formic acid and water (Thermo Fisher, Waltham, MA). The digests were loaded onto a reversed-phase trap column (Acclaim PepMap 100, 75 μm × 2 cm, nano viper, C18, 3 μm, 100 Å, Thermo Fisher, Waltham, MA) with an easyNanoLC 1200 (Thermo Fisher, Waltham, MA) for 10 μL at a flow rate of 5 μL/min. The trapped peptides were then analytically separated (Acclaim PepMap RSLC, 75 μm × 25 cm, 2 μm, 100 Å, Thermo Fisher, Waltham, MA) with a 120 min linear gradient of 7−32% buffer B (0.1% formic acid, 80% acetonitrile, 20% H_2O, Thermo Fisher, Waltham, MA) at a flow rate of 300 nL/min. The separated peptides were then electrosprayed in positive mode into a Fusion Lumos Tribrid mass spectrometer (Thermo Fisher, Waltham, MA). The mass spectrometry method has been previously outlined and is only briefly detailed here (Brown et al., submitted). The precursor ions were selected for higher energy collision dissociation (HCD) tandem mass analysis when there was an adequate signal (intensity threshold: 2.0 × 10^5) and their MH + mass was above 1500. The precursor ions with a z > 2 were set to a

https://dx.doi.org/10.1021/acs.analchem.0c01952
Anal. Chem. 2020, 92, 14357−14365

higher priority than those with a $z = 2$. The ions were isolated with a 0.5 m/z offset and an isolation window of 3 m/z, with the quadrupole analyzer. If during the MS2 using HCD, the ion fragmented to form an *N*-acetylglucosamine oxonium ion (m/z = 204.0867 Da), it is subsequently selected for activated ion electron transfer dissociation (EThcD). HCD collision energy was set to 35 ± 5%, while activation during EThcD was set to 15%. The ETD parameters were calibrated with angiotensin (Thermo Fisher, Waltham, MA). Both MS1 and MS2 spectra were detected in the Orbitrap mass analyzer at resolutions of 60 000 and 30 000, respectively. For HCD scans, the AGC was set to 2×10^5 ions with a maximum fill time of 150 ms, while for EThcD, the AGC was set to 1.5×10^5 ions with a maximum fill time of 200 ms. A dynamic exclusion window of 60 s was used to prevent reacquisition of the same precursor during this time.

Database Searching. Two database searching programs were used to separately identify the glycopeptides from the HCD spectra and EThcD spectra. The data from the nonenriched sample was analyzed by LC-MS and searched separately using Proteome Discoverer to determine the overall protein content of exosomes, and glycosylation was not allowed as a modification for that sample. For each search program, individual fractions from the lectin enrichment (ranging from retention volume ~39 to 48 mL in Figure 1D) were analyzed by LC-MS and the resulting data files were merged for a combined search. The peptides were searched against the *Homo sapiens* Uniprot proteome (Download Date: 2018-07-03), allowing for 2 missed cleavages. A parent mass tolerance of 5 ppm and a fragment ion tolerance of 20 ppm were used. Variable modifications included methionine oxidation, carbamidomethylated cysteine, Gln to pyro-Glu, N-term acetylation, N-term methionine loss, and N-term methionine loss plus acetylation. Glycans in the initial search were those present in the default list used by PGlyco. The results were then filtered using a list of 218 *N*-glycans identified by glycomic/glycoproteomic analyses of urinary exosomes[19,20] with a consensus motif of NXS/T, where X ≠ proline. An additional 13 glycan structures were also accepted due to their high-abundance identifications by EThcD and HCD as well as their close compositional relationship to accepted glycans (Supporting Information Table) to bring the total number of allowed glycans to 231. Of the 218 glycans found previously by glycomics, we identified glycopeptides bearing 128 of them in the current study. Protein Prospector (v 5.22.1) was used to search the EThcD spectra, allowing up to 3 modifications on each peptide. pGlyco 2.0 was used to search the HCD spectra. The scoring filters were applied to the data based on previous work, requiring a peptide expectation value less than 0.05 for Protein Prospector (for more details, see ref 21). For pGlyco 2.0, we required both the glycan and peptide scores to be >11 (for a discussion of the pGlyco scoring algorithm, see ref 22). pGlyco 2.0 generates a decoy sequence search along with the forward results, and applying these cutoff values resulted in an observed FDR less than 0.1%. For a subset of spectra around these cutoff values, we manually confirmed the spectra. The initial, nonenriched peptide sample was searched using Proteome Discoverer (version 2.1) using the same mass tolerances and nonglycan modifications as above. The Sequest HT algorithm was used to interpret the MS/MS spectra. The Percolator Node was used to filter the results with a maximum Delta Cn of 0.05 and a target FDR of 0.01. Unique and Razor peptides were used for protein level

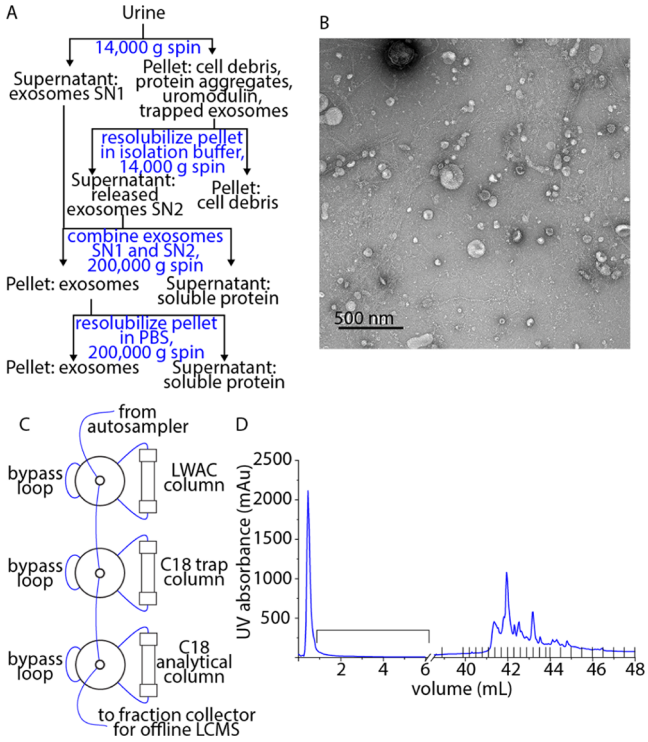

Figure 1. (A) Overview of the urinary exosome isolation procedure. Urine was subjected to a 14 000*g* spin. Most of the exosomes were removed in the supernatant and set aside. The exosomes trapped in the THP aggregates were resolubilized and isolated in a second 14 000*g* spin. These two exosome populations were pooled and pelleted in a 200 000*g* spin. (B) Electron micrograph of the resulting purified exosome sample. (C) Schematic of the glycopeptide enrichment HPLC setup. The lectin enrichment column, C18 trap column, and C18 analytical column were connected with a series of switching valves, which allowed the individual columns to be taken off-line. Initially, only the lectin column was in the flow-path and the early eluting peptides were diverted to waste. As the tail of the unbound fraction eluted, the C18 trap was placed online and weakly bound/late eluting glycopeptides were trapped. The total sample was injected in aliquots to prevent the overloading of the lectin column. After all glycopeptides were bound on the trap, the lectin column was taken out of the flow-path and the analytical column was placed in-line to fractionate the peptides. These fractions were then individually injected for LC-MS analysis. (D) LC trace of the final lectin enrichment showing the region of the gradient captured on the C18 trap. Also shown is the high pH RP gradient of the combined glycopeptides as they elute off the trap and are fractionated by the analytical column. The fractions were acquired from 40 to 50 mL into that gradient. Individual fraction locations are indicated by the vertical bars.

quantification. Following filtering, glycopeptide identifications were merged and aligned in Excel. Data analysis was carried out with OriginPro 2019 and Microsoft Excel. Gene ontology data were analyzed with DAVID Gene Ontology (v. 6.8, https://david.ncifcrf.gov). All. raw files and processed peaklists have been submitted to massive.ucsd.edu and are accessible at ftp://MSV000085965@massive.ucsd.edu. Data is accessible with the password: "CJB_2020.

Glycopeptide Quantification. For quantification of uromodulin peptides, extracted ion chromatograms were manually created using the Thermo Xcalibur Qual Browser. Identifications and MS/MS retention times from pGlyco and Protein Prospector were used to guide the extraction. For each

https://dx.doi.org/10.1021/acs.analchem.0c01952
Anal. Chem. 2020, 92, 14357−14365

glycopeptide, the monoisotopic mass with a window of ±100 ppm was used, and in the event that more than one elution peak was observed in a single run, the MS/MS retention time was used. The default automatic peak detection algorithm was used to calculate the peak areas. Individual glycopeptides were only quantified in the fraction, which produced the best scoring MS/MS spectra.

RESULTS AND DISCUSSION

Urinary exosomes were isolated by differential ultracentrifugation (Figure 1A). Electron microscopy was used to confirm that the exosomes were isolated in the expected mass range (Figure 1B). The proteins were digested with trypsin and the resulting peptides were enriched with a multilectin weak affinity chromatography (M-LWAC) column before being fractionated with a high pH reversed-phase analytical column (Figure 1C,D). This study identified 3144 unique glycosylation events from 378 glycoproteins (Supporting Information Table 1). A unique glycosylation event was defined as a unique glycan at a specific site on a given protein, and as such, redundant identifications of the same glycan/site (for example, due to missed cleavage variants) were not included in the number 3144. These glycopeptides were modified with a total of 141 unique glycan compositions, and they mapped to 604 unique sites on the list of proteins.

In addition to lectin enrichment and glycopeptide identification, we also characterized the overall urinary exosome proteome. This characterization allowed us to relate the number of glycosylated peptides identified to the underlying protein abundance (Figure 2). Figure 2A shows the relative abundance of each protein, estimated from its three

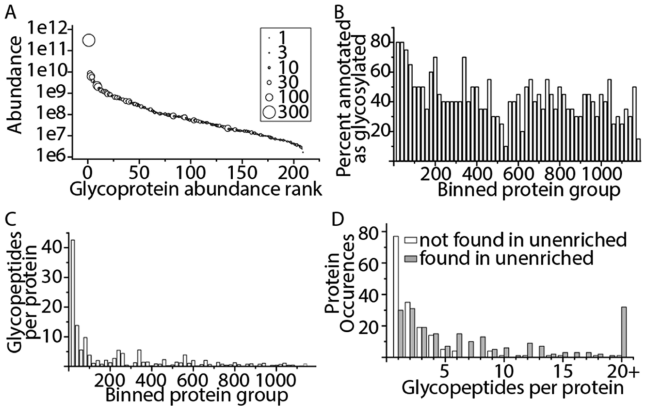

Figure 2. (A) Abundance of individual glycoproteins was plotted as a function of that protein's relative rank within the unenriched proteome, with the most abundant glycoproteins having the lowest rank. Each glycopeptide was shown as a circle whose diameter was proportional to the number of identified glycopeptides. (B) Proteins identified in the unenriched proteome analysis were grouped in bins of 20 by the relative abundance with the most abundant proteins to the left in the smallest bin group. For each bin, the percentage of proteins found to be glycosylated was calculated. For example, if 16 out of the 20 proteins in that bin were found glycosylated, the percentage would be 80%. (C) Same protein bins were used as in 2C and the average number of glycopeptides/protein in each bin was calculated. (D) Histogram representing the number of proteins that were found with a given number of glycopeptides. The white bars represent the subset of glycoproteins not detected in our analysis of the unenriched proteome, while the gray bars represent those glycoproteins that are also found in our unenriched analysis.

most intense peptides from the overall proteome MS1 data.[23,24] Proteins identified in both the overall proteome characterization as well as the glycopeptide analysis were rank-ordered as a function of protein abundance with a rank of "1" being the most abundant. Individual proteins were plotted as circles, whose diameters were proportional to the number of unique glycopeptides identified for that protein. Uromodulin, the most abundant protein, was identified with the largest number of unique glycopeptides, 389. Although there was a bias toward identifying more glycopeptides for higher abundance proteins, lower abundance proteins were not necessarily identified with only one or two glycopeptides. Of the glycoproteins whose abundance placed them in the 101st–200th rank for our sample, 48 of them were identified with a moderate amount of glycosylation (defined as five or more glycopeptides). Another notable glycoprotein identified in our studies was prostate-specific antigen (KLK3), which was the approximately 1% as abundant as uromodulin. We identified five unique glycopeptides mapping to two sites on this protein (Supporting Information Table 1).

To characterize the overall proteome, we determined the set of Uniprot human proteins annotated as being glycosylated and cross-referenced this information with our proteome quantification data. From the 1182 proteins we found in exosomes, 506 of them were annotated as glycoproteins (42%). We binned these data by abundance and plotted a histogram showing the relationship between exosome abundance and the fraction of proteins within a bin that were annotated as glycoproteins (Figure 2B). With the exception of a slight increase in frequency for the most abundant proteins, protein abundance did not predict the likelihood that a protein was a glycoprotein. Using the same bins, we investigated the average number of glycopeptides identified per protein as a function of protein abundance (Figure 2C). We observed a strong propensity for the 80 most abundant proteins to have large numbers of identified glycopeptides relative to the entire dataset. The fact that we found fewer glycopeptides for lower abundance proteins despite the fact that they are almost as likely to be glycosylated indicates likely limitations in the depth of our glycopeptide coverage. We then compared the distribution of glycopeptides per protein for those proteins found versus not found in the nonenriched proteome analysis (Figure 2D). Consistent with Figure 2C, those proteins not found in the nonenriched proteome analysis (which presumably represent low-abundance components) were found with many fewer glycopeptides per protein and mostly with a single glycopeptide. In contrast, those proteins found in the nonenriched proteome analysis were highly glycosylated, with 50% being identified with seven or more glycopeptides.

In addition to the proteins that were mapped to the urinary exosome proteome, we also identified many glycopeptides that mapped to proteins that were not identified in the unenriched exosomes (n = 164). The average number of glycopeptides used to identify each protein in this subgroup was lower (438 glycopeptides per 167 proteins or 2.7) relative to that of proteins observed in the unenriched dataset (2706 glycopeptides per 214 proteins, or 12.6). Proteins identified only after glycopeptide enrichment showed an increased level for the cellular compartment term "intrinsic to the membrane" (enrichment score: 3.65, p-value $<1.9 \times 10^{-4}$). In contrast, proteins observed in the overall exosome proteome showed an enrichment for the cellular compartment termed "lysosome"

https://dx.doi.org/10.1021/acs.analchem.0c01952
Anal. Chem. 2020, 92, 14357−14365

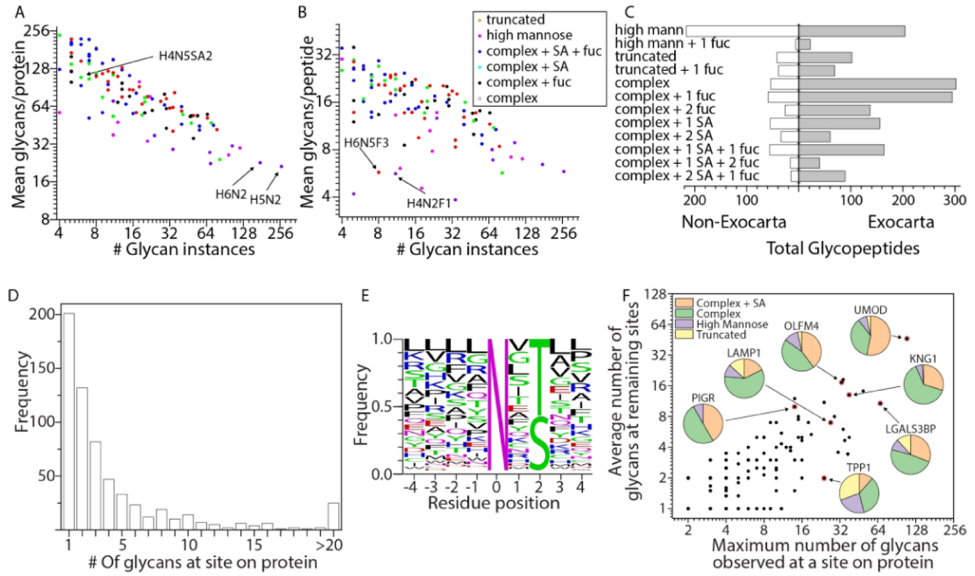

Figure 3. (A, B) For those glycans identified on four or more glycopeptides, a comparison of the number of glycopeptides identified bearing a given glycan versus the average number of glycans identified on those proteins (A) or peptides (B). As the number of times a glycan is found increases, the average glycosylation per protein/peptide decreases. Glycans such as Hex5HexNAc2 and Hex6HexNAc2 are highly abundant (as determined by glycomics[19]) and they are also found on proteins with high levels of identified glycans. They are the most common glycans found on proteins with low levels of identified glycopeptides, thus lowering their average. (C) Comparison of the types of glycopeptides identified as a function of whether the underlying proteins were annotated in Exocarta. Glycopeptides from proteins annotated as in Exocarta as exosomal (right side, gray bars) versus not previously annotated in Exocarta (left side, white bars). The size of each bar is proportional to the total observations of glycopeptides in a particular family. (D) Histogram showing the extent of microheterogeneity at each site of glycosylation across the dataset. (E) Calculated amino acid sequence motif around the modified asparagine residue for all identified glycopeptides. (F) Glycoprotein glycan heterogeneity is expressed as the maximum number of glycans observed at one site versus the average number of glycans at the remaining sites on the protein. Only proteins found with two or more identified sites were used for this analysis. The pie graphs for selected glycoproteins show the relative abundance of the glycans modifying that protein.

(enrichment score: 2.24, p-value $<4.2 \times 10^{-3}$). Exosomes have previously been shown to bud from both the endoplasmic reticulum as multivesicle bodies[25] and directly from the plasma membrane,[26] reinforcing the gene ontology descriptors described above.

For 66 proteins that have annotated glycosylation sites in Uniprot, we identified an additional 80 sites of glycosylation. We also identified 33 glycoproteins that were present in the Uniprot database, but which contained no annotations for sites of glycosylation. One example is Sec16A, which is involved in regulation of COPII-dependent endoplasmic reticulum vesicle budding in humans.[27−29] We observed previously unreported glycosylation on the secretory carrier-associated membrane protein (SCAMP1). This protein is involved in the post-Golgi vesicle-mediated transport with a possible role in exosome formation.[30] Importantly, the loss of this protein affects levels of the protein metastasis suppressor protein 1, which controls levels of cancer cell adhesion. The abundance of SCAMP1 leads to increased metastasis and poorer prognosis for breast and other cancers.[31,32]

Searching against a list of glycans largely comprised of those identified in large-scale glycomics/glycoproteomics analyses of human urine,[19,20] we identified 141 unique glycan compositions in the current analysis. Based upon glycan composition, we divided this population into high-mannose or complex/hybrid subsets. In the case of certain subunit compositions, it is possible to differentiate complex from hybrid glycans, but for a large percentage, this is not possible. Diagnostic ions in the HCD spectra may provide additional information to distinguish these classes,[33] but this has not been implemented in the pGlyco software. Within each subset, we parsed glycans based on the number of fucose or sialic acid residues. Glycans containing these two residue types have particular relevance considering their implications in disease.[34−36] Overall, we identify a diverse number of glycoforms with the largest group belonging to high-mannose type (n = 836), followed by complex (n = 588) and complex with a single fucosylation (n = 548). Of the 53 potential glycan structures that we did not identify, 28 of these were from glycans containing three or more sialic acid residues. This relatively limited detection of multiply-sialylated glycopeptides may result from the difficulties in effectively ionizing these species,[37] loss of sialic acid residues with our instrumentation,[38] multiply-sialylated glycans being present at low levels on many glycopeptides, or enrichment-specific biases.

To gain insight into the relationship between the observed glycan frequency and the types of sites found modified, for each instance that a given glycan was found on a glycopeptide, we calculated the average number of glycopeptides found on those proteins. We then plotted the total number of times a given glycan was identified versus the average glycosylation level on proteins that were glycan-modified (Figure 3A). In general, the more often a glycan was identified, the lower the average number of glycans were found on those proteins. Similarly, less common glycans were more likely to be found on more heterogeneous glycoproteins. The two most commonly identified glycans, HexNAc2Hex5 and HexNAc2Hex6 (263 and 176 identifications, respectively), are found on proteins bearing an average of 21.2 and 22.7 glycans, respectively. We repeated this analysis focusing on the average number of different glycans at each site rather than at the protein level (Figure 3B), and the overall trend of common

https://dx.doi.org/10.1021/acs.analchem.0c01952
Anal. Chem. 2020, 92, 14357−14365

glycans having a lower number of glycans per site still held. Taken as a whole, we interpret these results to indicate that more rarely identified glycans are found at lower frequencies due to the fact that they modify sites at low stoichiometry rather than being present at a smaller subset of sites. Analytical limitations in the analysis allow us to find these glycans only in the case of higher abundance proteins and/or highly ionizing peptides.

To further characterize our identified glycoproteins, we analyzed whether or not these proteins were listed in Exocarta (Figure 3C). The Exocarta database was developed to compile molecules identified in the published studies on exosomes.[39,40] For glycoproteins listed or not listed in Exocarta, we plotted the total number of glycopeptides identified that bore a given class of glycans. Interestingly, only the high-mannose family of glycoforms were found more often on proteins not annotated in Exocarta. Gene ontology analysis of these high-mannose, non-Exocarta proteins showed enrichment for the lysosome (enrichment score = 26.92, p-value $<5.4 \times 10^{-35}$), mirroring the subset of high-mannose proteins previously annotated as exosomal (lysosome term; enrichment score = 13.78, p-value $<2.8 \times 10^{-16}$). High-mannose glycans are among the most prevalent species modifying lysosomal membrane proteins,[41] although it is not necessarily the case that other tissues/organelles are not similarly enriched in high-mannose glycans. These proteins may be co-purified with the exosome preparation; however, the similarities in gene function to the known exosome-associated proteins suggest that these proteins are *bona fide* exosome components.

Identifying intact glycopeptides allows us to investigate the microheterogeneity of any site in our data. Recent work has shown that glycan microheterogeneity provides an important biological marker for different human diseases.[42−44] Overall, we observed 634 unique sites of glycosylation, with an average of approximately 5.0 glycans per site (Figure 3D). For all identified sites, we calculated the frequency of amino acids at each position (Figure 3E), noting the increased propensity of leucine residues at sites surrounding the glycosylated asparagine residue, which matches other work in the field.[12,16]

Protein glycosylation occurs both co- and post-translationally, often at multiple sites on a protein. Therefore, we wanted to estimate the extent to which the addition of specific glycans is regulated at the protein level as opposed to being regulated strictly by a local peptide sequence. To do so, we focused on proteins with more than one identified site of glycosylation. For each protein, the maximum number of glycoforms at a unique site on the protein was plotted relative to the average number of glycans at the remaining sites on those proteins (Figure 3F). There was a positive correlation between the protein level and peptide level microheterogeneity. This correlation suggests that the degree of microheterogeneity at individual sites is determined in part by the entire protein sequence/structure. To control for protein abundance affecting the level of observed microheterogeneity, we examined groups of proteins identified by varying amounts of glycopeptides and found that this trend was maintained.

Glycosylation on individual proteins provides relevant biological information with regard to protein structure,[45,46] adhesion,[47] and protein−protein interaction.[44] To investigate the extent to which individual proteins displayed various types of glycosylation patterns, we plotted the abundance of glycoform families in the highly glycosylated proteins in Figure 3F. These selected proteins displayed a range of glycosylation patterns, particularly with respect to the relative abundance of high-mannose and truncated glycans. Lysosomal-associated membrane protein 1 (LAMP1) and tripeptidyl-peptidase 1 (TPP1) showed a larger portion of truncated glycoforms, defined as glycans equal to or smaller than $GlcNAc_2Hex_3$, the chitobiose core. The source of truncated glycoforms is generally thought to originate from maturation/aging[48,49] or protein quality control measures.[50,51] In the case of LAMP1, changes in the amount of the larger sialylated glycoforms have recently been shown to affect cancer tumorigeneses.[52−54] Finally, although LGALS3BP (Mac-2 binding) is not directly associated with vacuole formation, it has been previously isolated with LAMP1[55] and also has implications in cancer tumorigenesis.[56]

The protein uromodulin (UMOD, Tamm−Horsfall Protein) was found to be heavily glycosylated. This abundant urine protein consists of roughly 20% carbohydrate by mass.[57,58] Our data provide evidence for glycosylation at five of the eight potential NXS/T sites throughout the protein backbone (Figure 4). The precise function of this protein is not well understood but is thought to be important for kidney and renal

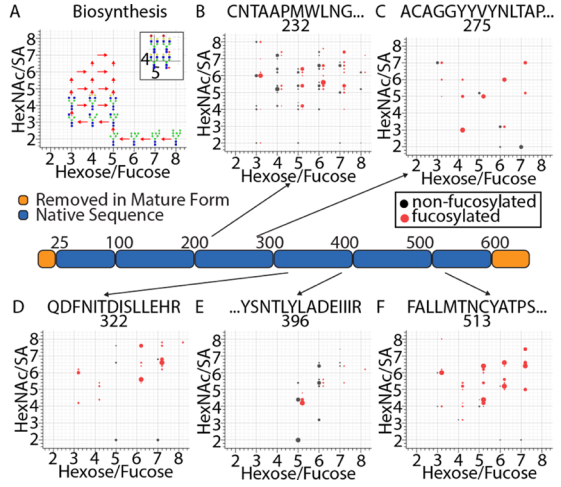

Figure 4. Tamm−Horsfall protein site-specific glycan microheterogeneity family abundance. Five sites of glycosylation on THP were characterized. (A) Graphical illustration of *N*-glycan biosynthesis arranged in an *XY* plot. Each glycoform was represented by a specific coordinate on the *XY* plot. The number of hexose residues was represented by an integer value along the *X*-axis and the number of fucose residues was represented by adding increments of 0.2 to the value for hexose. The number of HexNAc residues was represented by an integer value along the *Y* axis and the number of sialic acid residues was represented by adding increments of 0.2 to the value for HexNAc. The major gridlines are along integer values, so the circles at those positions represent glycans without fucose or sialic acid. The minor gridlines represent 0.2 increments, corresponding to fucose and sialic acid on the *X* and *Y* axis, respectively. The inset in the top right shows four glycan structures with the main composition HexNAc4Hex5 with (top) or without (bottom) an additional sialic acid or with (right) or without (left) an additional fucosylation. The search engines used do not distinguish between fucosylation of the core versus antenna. The circle diameters are proportional to the relative signal observed for that glycoform on a particular peptide. (B−F) Extracted ion chromatographs were used to determine relative MS abundances for each identified glycoform on the five sites of THP. In some cases, glycopeptides were identified by MS/MS, but the MS1-extracted ion chromatographs showed an insufficient signal for accurate quantification.

https://dx.doi.org/10.1021/acs.analchem.0c01952
Anal. Chem. 2020, 92, 14357−14365

function[57,59] and is annotated as exosomal. Glycosylation on this protein has been shown to control protein recognition between THP/uromodulin and other clinically relevant proteins.[60] THP glycosylation also functions in cellular recognition and has been shown to modulate immune cell activation.[61,62] Additionally, this protein also blocks against infection through the effective "coating" of pathogens' surfaces, thus preventing renal infections.[59] THP is by far the most heterogeneously glycosylated protein in our sample, with 131 of the 141 unique glycans in the overall sample being identified on at least one THP glycosylation site.

To obtain a granular view of the THP glycopeptide abundance, we determined the MS1 level signal for each THP glycopeptide by calculating the area of extracted ion chromatograms for each glycopeptide for the fraction in which it was detected (Figure 4). Each glycan contains up to four unique sugar subunits and hence four categories of quantitative data. We provide these data in a two-dimensional scatter plot by plotting the number of hexose units as integer values on the *X*-axis and the number of fucose residues as 0.2 increments from the hexose value. A more detailed description of this graphical nomenclature is the focus of a related manuscript (Trinidad et al., submitted). In a similar fashion, the number of HexNAc residues was plotted as an integer value on the *Y* axis, and the number of sialic acid residues was plotted in 0.2 increments from the HexNAc value. For example, a glycan with 6 hexoses, 4 HexNAc, 1 fucose, and 2 sialic acids would occur at position (*x*6.2, *y*4.4). For clarity, fucosylated glycans are colored red, whereas those lacking fucose are black. Figure 4A illustrates the relative position of those glycans involved in the initial steps from high-mannose to complex glycans, with arrows illustrating the biosynthetic route. The data from the five sites on THP look very different. For site 513, most of the glycans are sialylated and fucosylated, with a large percentage having 6/7 hexoses and 5/6 HexNAcs (Figure 4F). In contrast, sites 232 and 396 have a relatively higher percentage of glycans lacking fucose (Figure 4B,E). Site 275 appears to have the broadest distribution of glycans with respect to hexose and HexNAc composition. This representation of the data allows for a broad overview, understanding of how the main glycoforms at a given site are related biosynthetically, because any two locations, either 1.0 or 0.2 units apart, are likely related by a single synthetic step. The differential pattern at each site demonstrates that in the case of THP, the exact glycan distribution appears largely driven by the local chemical environment at each residue.

To determine the extent to which our identified glycopeptides have been previously characterized as potential prognostic cancer markers, we compared our results to data in the Protein Atlas (https://www.proteinatlas.org), as shown in Figure 5. The Protein Atlas includes a database of gene expression from tissues of healthy individuals as well as those suffering from specific cancers. The database identifies potential prognostic markers for 17 types of cancers. From our dataset of 3144 glycosylation events on 378 glycoproteins, 2096 glycopeptides from 248 glycoproteins were listed as prognostic markers for at least one cancer type and 1162 of our glycopeptides from 129 proteins matched to renal cancer markers. This finding translates to over half of all identified glycopeptides in the urinary exosomes mapping to proteins that are also annotated as prognostic markers in renal cancer (Figure 5B). Future work characterizing the glycosylation patterns on these proteins during disease would provide

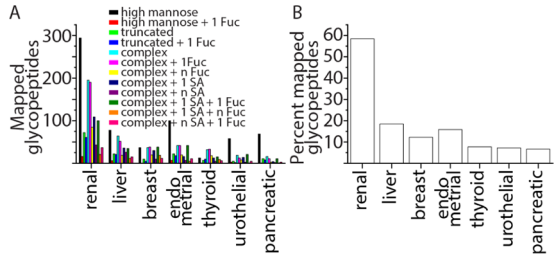

Figure 5. (A) For each of the glycopeptides identified, the percentage of proteins listed as potential prognostic cancer markers in Protein Atlas was calculated. The number of glycoforms identified on a peptide that mapped to a specific prognostic marker are provided. Prognostic marker mapping was completed with the Protein Atlas Project. (B) For all of the glycopeptides that mapped to a prognostic protein, the percentage of glycopeptides mapping to a specific cancer was calculated.

additional metrics to characterize this disease state since it certainly does not necessarily follow that if a given protein is a diagnostic than all or most glycosylation events on that protein are also diagnostic. Data in the Protein Atlas is based primarily on differences in RNA levels. Given the ability of the cancer cells to differentially glycosylate proteins, future work examining glycoform-specific variants of these proteins will be particularly informative.[42,63−66]

CONCLUSIONS

Exosomes represent a class of lipid-bound molecular transport vesicles, which are able to traverse long distances while retaining functional protein components. Protein glycosylation represents an important functional modality in both the sorting of cargo into these vesicle species[67] and the cellular targeting of released exosomes.[68] Therefore, glycoproteome analysis allows for a more detailed understanding of exosome physiology. This study observed 3144 glycosylation events originating from 378 glycoproteins. These proteins were diversely glycosylated with many peptides being glycosylated numerous times (average = 5.9 glycans/site). Furthermore, we observed differences in the glycan profiles at both the protein and the peptide level. This work represents an initial approach to study the glycosylation patterns on these important biological materials. The current study leveraged the glycomics results from our previous work,[13,19] in particular with respect to utilization of identified glycans to guide glycopeptide MS interpretation. These studies were highly complementary inasmuch as glycomics analysis can utilize chemical derivatization of released glycans to improve MS detection and facilitate in-depth structural characterization, an aspect that cannot be easily achieved in large-scale glycoproteomics studies.

ASSOCIATED CONTENT

Supporting Information

The Supporting Information is available free of charge at https://pubs.acs.org/doi/10.1021/acs.analchem.0c01952.

"Combined results" shows the aligned results of the pGlyco and Protein Prospector searches; "searched glycans" lists all of the glycans used in as variable modifications; "unique glycan site" shows the data removing redundancy (due to factors such as missed cleavages); "unique glycosylation array" formats the results as an array of unique protein sites versus glycans to indicate which combinations were identified; "label

https://dx.doi.org/10.1021/acs.analchem.0c01952
Anal. Chem. 2020, 92, 14357−14365

free quantification" shows the results of manual extracted ion chromatograph peak areas for THP glycopeptides (XLSX)

AUTHOR INFORMATION

Corresponding Authors

Jonathan C. Trinidad − *Department of Chemistry, Indiana University, Bloomington, Indiana 47401, United States;* orcid.org/0000-0002-8279-1509; Email: trinidad@indiana.edu

Milos V. Novotny − *Department of Chemistry, Indiana University, Bloomington, Indiana 47401, United States;* orcid.org/0000-0001-5530-7059; Email: novotny@indiana.edu

Authors

Christopher J. Brown − *Department of Chemistry, Indiana University, Bloomington, Indiana 47401, United States*

Stefan Gaunitz − *Department of Chemistry, Indiana University, Bloomington, Indiana 47401, United States*

Ziyu Wang − *Department of Chemistry, Indiana University, Bloomington, Indiana 47401, United States*

Lena Strindelius − *Department of Chemistry, Indiana University, Bloomington, Indiana 47401, United States*

Stephen C. Jacobson − *Department of Chemistry, Indiana University, Bloomington, Indiana 47401, United States;* orcid.org/0000-0003-2415-041X

David E. Clemmer − *Department of Chemistry, Indiana University, Bloomington, Indiana 47401, United States;* orcid.org/0000-0003-4039-1360

Complete contact information is available at: https://pubs.acs.org/10.1021/acs.analchem.0c01952

Notes

The authors declare no competing financial interest.

ACKNOWLEDGMENTS

This work was supported by the National Institutes of Health Grant number 5R01GM117207 (D.E.C.), K01 MH107756 (M.V.N.), NIH R01 GM106084 (S.C.J.), and Indiana University Precision Health Grand Challenge Initiative (J.C.T.).

REFERENCES

(1) Tominaga, N.; Kosaka, N.; Ono, M.; Katsuda, T.; Yoshioka, Y.; Tamura, K.; Lotvall, J.; Nakagama, H.; Ochiya, T. *Nat. Commun.* **2015**, *6*, No. 6716.

(2) Royo, F.; Cossio, U.; Ruiz de Angulo, A.; Llop, J.; Falcon-Perez, J. M. *Nanoscale* **2019**, *11*, 1531−1537.

(3) Deatherage, B. L.; Cookson, B. T. *Infect. Immun.* **2012**, *80*, 1948−1957.

(4) Teng, Y.; Ren, Y.; Sayed, M.; Hu, X.; Lei, C.; Kumar, A.; Hutchins, E.; Mu, J.; Deng, Z.; Luo, C.; Sundaram, K.; Sriwastva, M. K.; Zhang, L.; Hsieh, M.; Reiman, R.; Haribabu, B.; Yan, J.; Jala, V. R.; Miller, D. M.; Van Keuren-Jensen, K.; et al. *Cell Host Microbe* **2018**, *24*, 637−652.

(5) Alvarez-Erviti, L.; Seow, Y.; Yin, H.; Betts, C.; Lakhal, S.; Wood, M. J. *Nat. Biotechnol.* **2011**, *29*, 341−345.

(6) Aryani, A.; Denecke, B. *Mol. Neurobiol.* **2016**, *53*, 818−834.

(7) Baker, E. S.; Burnum-Johnson, K. E.; Jacobs, J. M.; Diamond, D. L.; Brown, R. N.; Ibrahim, Y. M.; Orton, D. J.; Piehowski, P. D.; Purdy, D. E.; Moore, R. J.; Danielson, W. F., 3rd; Monroe, M. E.; Crowell, K. L.; Slysz, G. W.; Gritsenko, M. A.; Sandoval, J. D.; Lamarche, B. L.; Matzke, M. M.; Webb-Robertson, B. J.; Simons, B. C.; et al. *Mol. Cell. Proteomics* **2014**, *13*, 1119−1127.

(8) Iaccino, E.; Mimmi, S.; Dattilo, V.; Marino, F.; Candeloro, P.; Di Loria, A.; Marimpietri, D.; Pisano, A.; Albano, F.; Vecchio, E.; Ceglia, S.; Golino, G.; Lupia, A.; Fiume, G.; Quinto, I.; Scala, G. *Mol. Cancer* **2017**, *16*, 159.

(9) San Lucas, F. A.; Allenson, K.; Bernard, V.; Castillo, J.; Kim, D. U.; Ellis, K.; Ehli, E. A.; Davies, G. E.; Petersen, J. L.; Li, D.; Wolff, R.; Katz, M.; Varadhachary, G.; Wistuba, I.; Maitra, A.; Alvarez, H. *Ann. Oncol.* **2016**, *27*, 635−641.

(10) Köttgen, A.; Hwang, S. J.; Larson, M. G.; Van Eyk, J. E.; Fu, Q.; Benjamin, E. J.; Dehghan, A.; Glazer, N. L.; Kao, W. H.; Harris, T. B.; Gudnason, V.; Shlipak, M. G.; Yang, Q.; Coresh, J.; Levy, D.; Fox, C. S. *J. Am. Soc. Nephrol.* **2010**, *21*, 337−344.

(11) Desaire, H. *Mol. Cell. Proteomics* **2013**, *12*, 893−901.

(12) Riley, N. M.; Hebert, A. S.; Westphall, M. S.; Coon, J. J. *Nat. Commun.* **2019**, *10*, No. 1311.

(13) Zou, G.; Benktander, J. D.; Gizaw, S. T.; Gaunitz, S.; Novotny, M. V. *Anal. Chem.* **2017**, *89*, 5364−5372.

(14) Kang, P.; Madera, M.; Alley, W. R., Jr.; Goldman, R.; Mechref, Y.; Novotny, M. V. *Int. J. Mass Spectrom.* **2011**, *305*, 185−198.

(15) Alley, W. R., Jr.; Mann, B. F.; Novotny, M. V. *Chem. Rev.* **2013**, *113*, 2668−2732.

(16) Zielinska, D. F.; Gnad, F.; Wisniewski, J. R.; Mann, M. *Cell* **2010**, *141*, 897−907.

(17) Nicastri, A.; Gaspari, M.; Sacco, R.; Elia, L.; Gabriele, C.; Romano, R.; Rizzuto, A.; Cuda, G. *J. Proteome Res.* **2014**, *13*, 4932−4941.

(18) Wiśniewski, J. R. *Anal. Chem.* **2016**, *88*, 5438−5443.

(19) Song, W.; Zhou, X.; Benktander, J. D.; Gaunitz, S.; Zou, G.; Wang, Z.; Novotny, M. V.; Jacobson, S. C. *Anal. Chem.* **2019**, *91*, 13528−13537.

(20) Saraswat, M.; Joenvaara, S.; Musante, L.; Peltoniemi, H.; Holthofer, H.; Renkonen, R. *Mol. Cell. Proteomics* **2015**, *14*, 263−276.

(21) Trinidad, J. C.; Schoepfer, R.; Burlingame, A. L.; Medzihradszky, K. F. *Mol. Cell. Proteomics* **2013**, *12*, 3474−3488.

(22) Liu, M. Q.; Zeng, W. F.; Fang, P.; Cao, W. Q.; Liu, C.; Yan, G. Q.; Zhang, Y.; Peng, C.; Wu, J. Q.; Zhang, X. J.; Tu, H. J.; Chi, H.; Sun, R. X.; Cao, Y.; Dong, M. Q.; Jiang, B. Y.; Huang, J. M.; Shen, H. L.; Wong, C. C. L.; He, S. M.; et al. *Nat. Commun.* **2017**, *8*, No. 438.

(23) Silva, J. C.; Gorenstein, M. V.; Li, G. Z.; Vissers, J. P.; Geromanos, S. J. *Mol. Cell. Proteomics* **2006**, *5*, 144−156.

(24) Silva, J. C.; Denny, R.; Dorschel, C. A.; Gorenstein, M.; Kass, I. J.; Li, G. Z.; McKenna, T.; Nold, M. J.; Richardson, K.; Young, P.; Geromanos, S. *Anal. Chem.* **2005**, *77*, 2187−2200.

(25) Christ, L.; Raiborg, C.; Wenzel, E. M.; Campsteijn, C.; Stenmark, H. *Trends Biochem. Sci.* **2017**, *42*, 42−56.

(26) Gan, X.; Gould, S. J. *Mol. Biol. Cell* **2011**, *22*, 817−830.

(27) Hughes, H.; Budnik, A.; Schmidt, K.; Palmer, K. J.; Mantell, J.; Noakes, C.; Johnson, A.; Carter, D. A.; Verkade, P.; Watson, P.; Stephens, D. J. *J. Cell Sci.* **2009**, *122*, 2924−2934.

(28) Kurokawa, K.; Nakano, A. *J. Biochem.* **2019**, *165*, 109−114.

(29) Yorimitsu, T.; Sato, K. *Mol. Biol. Cell* **2012**, *23*, 2930−2942.

(30) Fernández-Chacón, R.; Alvarez de Toledo, G.; Hammer, R. E.; Sudhof, T. C. *J. Biol. Chem.* **1999**, *274*, 32551−32554.

(31) Vadakekolathu, J.; Al-Juboori, S. I. K.; Johnson, C.; Schneider, A.; Buczek, M. E.; Di Biase, A.; Pockley, A. G.; Ball, G. R.; Powe, D. G.; Regad, T. *Cell Death Dis.* **2018**, *9*, 344.

(32) Biewenga, P.; Buist, M. R.; Moerland, P. D.; Ver Loren van Themaat, E.; van Kampen, A. H.; ten Kate, F. J.; Baas, F. *Gynecol. Oncol.* **2008**, *108*, 520−526.

(33) Rouse, J. C.; Strang, A. M.; Yu, W.; Vath, J. E. *Anal. Biochem.* **1998**, *256*, 33−46.

(34) Okuyama, N.; Ide, Y.; Nakano, M.; Nakagawa, T.; Yamanaka, K.; Moriwaki, K.; Murata, K.; Ohigashi, H.; Yokoyama, S.; Eguchi, H.; Ishikawa, O.; Ito, T.; Kato, M.; Kasahara, A.; Kawano, S.; Gu, J.; Taniguchi, N.; Miyoshi, E. *Int. J. Cancer* **2006**, *118*, 2803−2808.

(35) Kawahara, R.; Ortega, F.; Rosa-Fernandes, L.; Guimaraes, V.; Quina, D.; Nahas, W.; Schwammle, V.; Srougi, M.; Leite, K. R. M.;

Thaysen-Andersen, M.; Larsen, M. R.; Palmisano, G. *Oncotarget* **2018**, *9*, 33077−33097.
(36) Alley, W. R., Jr.; Vasseur, J. A.; Goetz, J. A.; Svoboda, M.; Mann, B. F.; Matei, D. E.; Menning, N.; Hussein, A.; Mechref, Y.; Novotny, M. V. *J. Proteome Res.* **2012**, *11*, 2282−2300.
(37) Fukuyama, Y.; Nakaya, S.; Yamazaki, Y.; Tanaka, K. *Anal. Chem.* **2008**, *80*, 2171−2179.
(38) Weiskopf, A. S.; Vouros, P.; Harvey, D. J. *Anal. Chem.* **1998**, *70*, 4441−4447.
(39) Keerthikumar, S.; Chisanga, D.; Ariyaratne, D.; Al Saffar, H.; Anand, S.; Zhao, K.; Samuel, M.; Pathan, M.; Jois, M.; Chilamkurti, N.; Gangoda, L.; Mathivanan, S. *J. Mol. Biol.* **2016**, *428*, 688−692.
(40) Simpson, R. J.; Kalra, H.; Mathivanan, S. *J. Extracell. Vesicles* **2012**, 1.
(41) Kosicek, M.; Gudelj, I.; Horvatic, A.; Jovic, T.; Vuckovic, F.; Lauc, G.; Hecimovic, S. *Mol. Cell. Proteomics* **2018**, *17*, 631−642.
(42) Miyamoto, S.; Stroble, C. D.; Taylor, S.; Hong, Q.; Lebrilla, C. B.; Leiserowitz, G. S.; Kim, K.; Ruhaak, L. R. *J. Proteome Res.* **2018**, *17*, 222−233.
(43) Kyselova, Z.; Mechref, Y.; Al Bataineh, M. M.; Dobrolecki, L. E.; Hickey, R. J.; Vinson, J.; Sweeney, C. J.; Novotny, M. V. *J. Proteome Res.* **2007**, *6*, 1822−1832.
(44) Wu, D.; Struwe, W. B.; Harvey, D. J.; Ferguson, M. A. J.; Robinson, C. V. *Proc. Natl. Acad. Sci. U.S.A.* **2018**, *115*, 8763−8768.
(45) Arnold, J. N.; Wormald, M. R.; Sim, R. B.; Rudd, P. M.; Dwek, R. A. *Annu. Rev. Immunol.* **2007**, *25*, 21−50.
(46) Hebert, D. N.; Lamriben, L.; Powers, E. T.; Kelly, J. W. *Nat. Chem. Biol.* **2014**, *10*, 902−910.
(47) Pinho, S. S.; Reis, C. A. *Cancer* **2015**, *15*, 540−555.
(48) Yang, W. H.; Aziz, P. V.; Heithoff, D. M.; Mahan, M. J.; Smith, J. W.; Marth, J. D. *Proc. Natl. Acad. Sci. U.S.A.* **2015**, *112*, 13657−13662.
(49) O'Sullivan, J. M.; Aguila, S.; McRae, E.; Ward, S. E.; Rawley, O.; Fallon, P. G.; Brophy, T. M.; Preston, R. J.; Brady, L.; Sheils, O.; Chion, A.; O'Donnell, J. S. *J. Thromb. Haemostasis* **2016**, *14*, 2446−2457.
(50) Hosokawa, N.; Kamiya, Y.; Kamiya, D.; Kato, K.; Nagata, K. *J. Biol. Chem.* **2009**, *284*, 17061−17068.
(51) Cabral, C. M.; Liu, Y.; Sifers, R. N. *Trends Biochem. Sci.* **2001**, *26*, 619−624.
(52) Cocucci, E.; Meldolesi, J. *Trends Cell Biol.* **2015**, *25*, 364−372.
(53) Krishnan, V.; Bane, S. M.; Kawle, P. D.; Naresh, K. N.; Kalraiya, R. D. *Clin. Exp. Metastasis* **2005**, *22*, 11−24.
(54) Agarwal, A. K.; Gude, R. P.; Kalraiya, R. D. *Biochem. Biophys. Res. Commun.* **2014**, *449*, 332−337.
(55) Przybylo, M.; Martuszewska, D.; Pochec, E.; Hoja-Lukowicz, D.; Litynska, A. *Biochim. Biophys. Acta, Gen. Subj.* **2007**, *1770*, 1427−1435.
(56) Weng, L. P.; Wu, C. C.; Hsu, B. L.; Chi, L. M.; Liang, Y.; Tseng, C. P.; Hsieh, L. L.; Yu, J. S. *J. Proteome Res.* **2008**, *7*, 3765−3775.
(57) Serafini-Cessi, F.; Malagolini, N.; Cavallone, D. *Am. J. Kidney Dis.* **2003**, *42*, 658−676.
(58) van Rooijen, J. J.; Voskamp, A. F.; Kamerling, J. P.; Vliegenthart, J. F. *Glycobiology* **1999**, *9*, 21−30.
(59) Coady, A.; Ramos, A. R.; Olson, J.; Nizet, V.; Patras, K. A. *Infect. Immun.* **2018**, 86.
(60) Wu, C. H.; Li, K. J.; Siao, S. C.; Chen, Y. H.; Wu, T. H.; Tsai, C. Y.; Yu, C. L. *Molecules* **2012**, *17*, 11978−11989.
(61) Rhodes, D. C. J. *PLoS One* **2017**, *12*, No. e0181857.
(62) Patras, K. A.; Coady, A.; Olson, J.; Ali, S. R.; RamachandraRao, S. P.; Kumar, S.; Varki, A.; Nizet, V. *Immunol. Cell Biol.* **2017**, *95*, 960−965.
(63) Veillon, L.; Fakih, C.; Abou-El-Hassan, H.; Kobeissy, F.; Mechref, Y. *ACS Chem. Neurosci.* **2018**, *9*, 51−72.
(64) Zhao, J.; Qiu, W.; Simeone, D. M.; Lubman, D. M. *J. Proteome Res.* **2007**, *6*, 1126−1138.
(65) de Leoz, M. L.; Young, L. J.; An, H. J.; Kronewitter, S. R.; Kim, J.; Miyamoto, S.; Borowsky, A. D.; Chew, H. K.; Lebrilla, C. B. *Mol. Cell. Proteomics 10* **2011**, *M110*, No. 002717.
(66) Tan, M.; Zhu, L.; Zhuang, H.; Hao, Y.; Gao, S.; Liu, S.; Liu, Q.; Liu, D.; Liu, J.; Lin, B. *Am. J. Cancer Res.* **2015**, *5*, 2777−2787.
(67) Liang, Y.; Eng, W. S.; Colquhoun, D. R.; Dinglasan, R. R.; Graham, D. R.; Mahal, L. K. *J. Biol. Chem.* **2014**, *289*, 32526−32537.
(68) Escrevente, C.; Keller, S.; Altevogt, P.; Costa, J. *BMC Cancer* **2011**, *11*, 108.

https://dx.doi.org/10.1021/acs.analchem.0c01952
Anal. Chem. 2020, 92, 14357−14365